# Fast Reconstruction for Multichannel Compressed Sensing Using a Hierarchically Semiseparable Solver

Stephen F. Cauley,[1]* Yuanzhe Xi,[2] Berkin Bilgic,[1,3] Jianlin Xia,[2] Elfar Adalsteinsson,[1,4] Venkataramanan Balakrishnan,[5] Lawrence L. Wald,[1,3,4] and Kawin Setsompop[1,3]

**Purpose:** The adoption of multichannel compressed sensing (CS) for clinical magnetic resonance imaging (MRI) hinges on the ability to accurately reconstruct images from an undersampled dataset in a reasonable time frame. When CS is combined with SENSE parallel imaging, reconstruction can be computationally intensive. As an alternative to iterative methods that repetitively evaluate a forward CS+SENSE model, we introduce a technique for the fast computation of a compact inverse model solution.

**Methods:** A recently proposed hierarchically semiseparable (HSS) solver is used to compactly represent the inverse of the CS+SENSE encoding matrix to a high level of accuracy. To investigate the computational efficiency of the proposed *HSS-Inverse* method, we compare reconstruction time with the current state-of-the-art. In vivo 3T brain data at multiple image contrasts, resolutions, acceleration factors, and number of receive channels were used for this comparison.

**Results:** The *HSS-Inverse* method allows for $>6\times$ speedup when compared to current state-of-the-art reconstruction methods with the same accuracy. Efficient computational scaling is demonstrated for CS+SENSE with respect to image size. The *HSS-Inverse* method is also shown to have minimal dependency on the number of parallel imaging channels/acceleration factor.

**Conclusions:** The proposed *HSS-Inverse* method is highly efficient and should enable real-time CS reconstruction on standard MRI vendors' computational hardware. **Magn Reson Med 73:1034–1040, 2015. © 2014 Wiley Periodicals, Inc.**

**Key words:** parallel imaging; compressed sensing; SENSE; hierarchically semiseparable

## INTRODUCTION

In clinical applications of structural magnetic resonance imaging (MRI), there exists a multiobjective trade-off between image quality, imaging time, and reconstruction time. Reducing imaging time for a given protocol is clearly beneficial from a cost perspective, and can also facilitate more detailed studies with the same patient throughput. Image quality tends to be a firm barrier placed by radiologists or researchers based on requirements for data analysis. Finally, stringent hardware limitations exist for clinical FDA approved scanners. It is important to note that advances in MRI sequences and hardware continue to increase the computational burden for image reconstruction, e.g., large coil arrays, increased resolution, and multicontrast studies. In this work, we investigate a highly scalable inverse algorithm intended to ameliorate the computational challenges associated with accurate compressed sensing (CS) reconstruction. As an alternative to reconstruction methods that repetitively evaluate forward CS/parallel imaging models, we introduce a technique for the computation of a compact inverse model solution. This is achieved by using a recently proposed hierarchically semiseparable (HSS) solver (1), which compactly represents the inverse encoding matrix to a high level of accuracy. Specifically, using a prespecified level of accuracy the HSS solver will systematically compress parameters from a decomposition of the encoding matrix. When solving a two-dimensional (2D) inverse encoding problem with $N$ voxels, even optimized Cholesky decomposition-based solvers such as (2) will require $\mathcal{O}(N^{1.5})$ computation in the best case. When the encoding matrix has certain low-rank properties, the HSS method can achieve $\mathcal{O}(N)$. Under these conditions, the HSS scaling is less than the fast Fourier transform (FFT) complexity of $\mathcal{O}(N\log N)$ while the optimized Cholesky is greater.

Sparse signal reconstruction has been introduced for MRI (3) as a method to improve imaging time through random undersampling of k-space. By assuming a sparsity inducing $\mathcal{L}_1$ image prior, the reconstruction problem can be formulated as an unconstrained optimization problem. This problem incorporates fidelity against the observed k-space samples with a penalty imposed on the sparsity prior. These methods have been shown to provide good image accuracy, but can significantly increase the computational burden for image reconstruction. This is especially evident with the inclusion of SENSE parallel imaging (4). Several attempts have been made to reduce the computational requirements associated with sparse signal reconstruction (5–11). These iterative techniques rely on repetitive evaluation of a forward

[1]Athinoula A. Martinos Center for Biomedical Imaging, Department of Radiology, Massachusetts General Hospital, Charlestown, Massachusetts, USA.
[2]Department of Mathematics, Purdue University, West Lafayette, Indiana, USA.
[3]Department of Radiology, Harvard Medical School, Boston, Massachusetts, USA.
[4]Harvard-MIT Division of Health Sciences and Technology, MIT, Cambridge, Massachusetts, USA.
[5]School of Electrical and Computer Engineering, Purdue University, West Lafayette, Indiana, USA.

Grant sponsor: NIH; Grant number: U01MH093765; Grant sponsor: NIBIB; Grant numbers: R00EB012107; R01EB006847; Grant sponsor: NCRR; Grant number: P41RR014075; Grant sponsor: NSF; Grant numbers: DMS-1255416; DMS-1115572; CHE-0957024.

*Correspondence to: Stephen F Cauley, Ph.D.; MGH Martinos Center for Biomedical Imaging, 149 13th Street, Rm 2301, Charlestown, MA 02129. E-mail: stcauley@nmr.mgh.harvard.edu

Received 6 January 2014; revised 21 February 2014; accepted 24 February 2014

DOI 10.1002/mrm.25222
Published online 17 March 2014 in Wiley Online Library (wileyonlinelibrary.com).

CS+SENSE model. In this work, we propose an alternative approach that solves for the actual inverse of the encoding matrix using a direct (noniterative) HSS solver.

To demonstrate the advantages of our *HSS-Inverse* approach we will focus on the popular split Bregman (SB) (8) formulation. Here, the authors presented a relaxation method for $\mathcal{L}_1$ penalties. The iterative SB approach produces a series of targets for the sparsity of the image. Each stage of the method involves solving an easier $\mathcal{L}_2$ optimization and quickly updating the sparsity target. Our *HSS-Inverse* solver and several iterative conjugate gradient (CG) approaches are embedded within the SB formulation for comparison. This allows for us to isolate the efficiency of solving the CS+SENSE model across consistent optimization problems. To accurately compare our method to state-of-the-art techniques, we will ensure optimized CG performance through the use of Jacobi preconditioning (9) and geometric coil compression (11) where applicable.

In this work, we empirically verify the linear computational scaling shown in Ref. (1) with respect to the size of the system being solved. The linear scaling is demonstrated through CS+SENSE reconstructions across multiple image resolutions, based on 32-channel 3T acquisitions. Specifically, our *HSS-Inverse* approach scales efficiently with the number of imaging voxels and minimizes the influence of acceleration factor/the number of parallel imaging channels toward the reconstruction time. This results in >6× speedup over iterative methods even when they take advantage of state-of-the-art preconditioning (9) and coil compression (11) techniques.

## THEORY

As described in Ref. (3), CS reconstruction involves solving an inverse problem in order to match an observed subset of data under an assumed sparsity prior. Here, MR images are assumed to be sparse or compressible under a total variation (TV) and/or wavelet transformation. We begin by briefly reviewing optimization methods for CS reconstruction. We will then summarize the application of iterative CG-based approaches and our *HSS-Inverse* technique within the reconstruction framework.

### CS with Total Variation Penalty

The CS formulation for MRI, as presented in Ref. (3), is an unconstrained optimization problem involving penalty terms based on assumed TV and wavelet sparsity. By predefining penalty weights $\alpha$ and $\gamma$, the CS optimization estimates the true image $x \in \mathbb{C}^N$:

$$\hat{x} = \arg\min_x \| F_\Omega x - y \|_2^2 + \alpha \| \Psi^T x\|_1 + \gamma TV(x). \quad [1]$$

Here, $F_\Omega \in \mathbb{C}^{M\times N}$ is the undersampled Fourier operator that transforms the image $x$ into k-space to match the observations $y \in \mathbb{C}^M$. Therefore, the acceleration factor is $R = N/M$. The data fidelity is measured using the $\mathcal{L}_2$ metric to represent root mean squared error (RMSE) against the observations. $\Psi$ is the wavelet transform that is applied to the image $x$ and the $\mathcal{L}_1$ metric is used to promote sparsity in that domain. Similarly, the TV operator computes a finite difference across the image $x$ to promote sparsity in this spatial smoothness domain. In this work, we will focus on the more general parallel imaging problem and for ease of illustration only consider TV sparsity. By introducing complex coil sensitivity profiles $\{C_i\}_{i=1,K}$, the SENSE parallel imaging model can be incorporated into the CS formulation (5,7,10):

$$\hat{x} = \arg\min_x \sum_{i=1}^{K} \|F_\Omega C_i x - y_i\|_2^2 + \gamma(\| G_v x\|_1 + \| G_h x\|_1). \quad [2]$$

Note that the TV operator has been rewritten as a sum of horizontal and vertical finite difference operators $G_h$ and $G_v$. The SB approach from (8) relaxes the $\mathcal{L}_1$ penalties through the iterative construction of $\mathcal{L}_2$ targets:

$$\begin{aligned}\hat{x} = \arg\min_x & \sum_{i=1}^{K} \|F_\Omega C_i x - y_i\|_2^2 \\ & + \beta\left(\| G_v x - g_v\|_2^2 + \| G_h x - g_h\|_2^2\right).\end{aligned} \quad [3]$$

The targets $g_v$ and $g_h$ can be updated simply using a soft thresholding truncation parameter $\varepsilon$. For example, $g_v \leftarrow \max(|G_v x| - \varepsilon/2, 0)\text{sign}(G_v x)$. This operation is linear time and thus the computational cost is dependent on the quadratic minimization shown in (3). The explicit solution of this minimization problem is:

$$\begin{aligned}&\left[\underbrace{\sum_{i=1}^{K} C_i^H F_\Omega^H F_\Omega C_i}_{T_F} + \beta \underbrace{\left(G_v^H G_v + G_h^H G_h\right)}_{T_S}\right] x \\ &= \underbrace{\sum_{i=1}^{K} C_i^H F_\Omega^H y_i + G_v^H g_v + G_h^H g_h}_{b}.\end{aligned} \quad [4]$$

Here, we denote $T_F$ as the Fourier operator which has been combined with the Laplacian operator $T_S$. We will refer to the inverse problem as the solution of $\underbrace{(T_F + \beta T_S)}_{A} x = b$ or evaluating $x = A^{-1}b$. It is important to note that $T_F, T_S$, and the parameter $\beta$ are constant with respect to the SB iteration and only depend on the protocol and coil sensitivity maps.

Figure 1 shows the flow diagram for three possible reconstruction scenarios. The *Matrix Free* and *Matrix* implementations (12) utilize an iterative CG-based solver and the direct HSS solver (1) is used for our proposed *HSS-Inverse* method. As can be seen in Figure 1, the CG-based methods require an evaluation of the forward CS+SENSE operator. For the *Matrix Free* method, the operator $A$ is evaluated by looping across all coils and performing FFT/sensitivity operations. Alternatively, the *Matrix* method directly computes the operator $A$ and removes this dependency on the number of parallel imaging channels. With the incorporation of channel compression techniques, the dependency of *Matrix Free* methods on the number of parallel channels can be

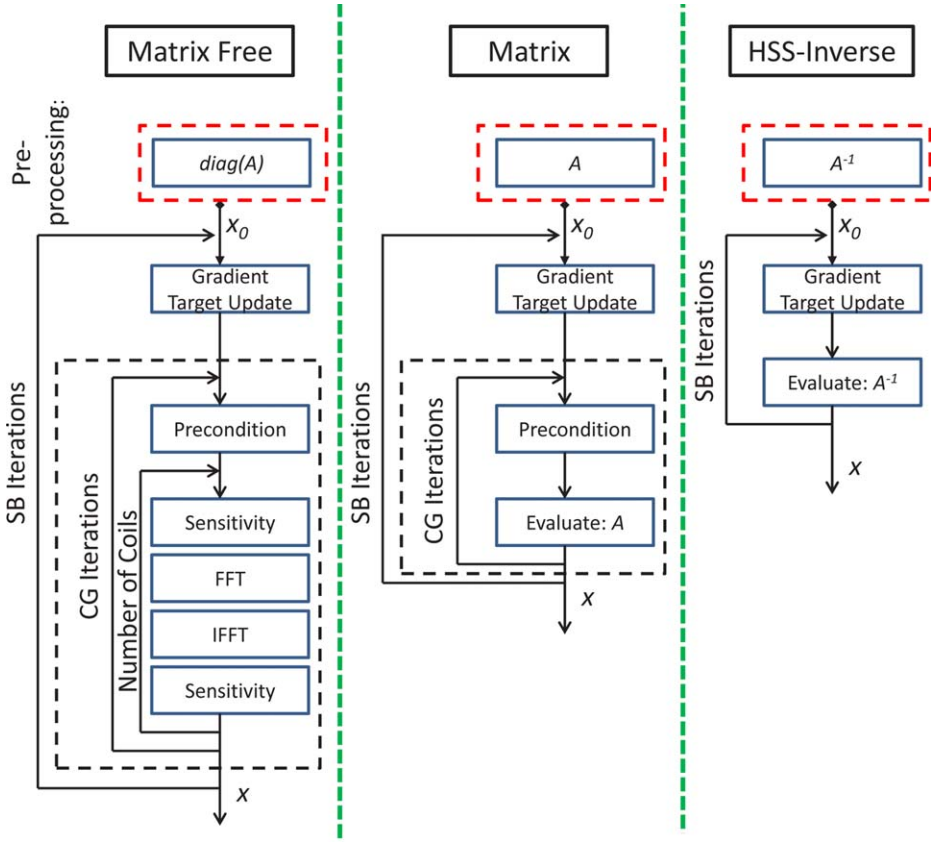


FIG. 1. SB CS+SENSE implementations are illustrated. The required precomputation is shown above the corresponding flow diagrams. The *Matrix Free* and *Matrix* methods rely on iterative CG solutions, while the *HSS-Inverse* method gives a direct solution for each SB iteration. The CG-based approaches are optimized with the diagonal Jacobi preconditioner.

reduced. Specifically, for the large array coils and Cartesian sampling used in this work, geometric coil compression (11) can be effectively used with only small loss in reconstruction accuracy. In the case of our *HSS-Inverse* method, a compact representation for the inverse operator $A^{-1}$ is formed using the HSS linear solver. This is accomplished by performing a structured factorization of the matrix $A$ into lower diagonal $L$ and diagonal $D$ components: $A = LDL^H$. Here, many of the terms in $L$ can either be inverted easily or represented using low-rank modeling. This allows for efficient evaluation of the inverse model.

The impact of hierarchical compression can be clearly seen when comparing the HSS solver to optimized Cholesky-based methods such as CHOLMOD (2). Figure 2 shows the computational scaling of the algorithms with respect to image size. Here, the size of the matrix corresponds to the number of voxels in the 2D images, which range from $112 \times 112$ to $448 \times 448$. To put this in perspective, the largest image has 200K voxels and an explicit representation of the dense matrix $A^{-1}$ would require over 600GB of memory to describe the $40 \times 10^9$ entries. Even if this matrix could be explicitly formed, the numerical evaluation would be extremely slow with a scaling of $\mathcal{O}(N^2)$. Alternatively, the representations for $A^{-1}$ using CHOLMOD and HSS are much more compact and computationally efficient. The inverse evaluation time is shown for CHOLMOD and the HSS solver using a $10^{-6}$ tolerance across several relevant image sizes. The matrices are associated with a $R = 3$ acceleration and 32 receive channels. The difference between the $\mathcal{O}(N^{1.5})$ scaling of CHOLMOD and the $\mathcal{O}(N)$ scaling of the HSS solver can be clearly observed. It is important to note that our HSS solver is implemented in MATLAB and the CHOLMOD solver we compared against is a highly optimized C++ implementation of (2). It is expected that a highly optimized C++

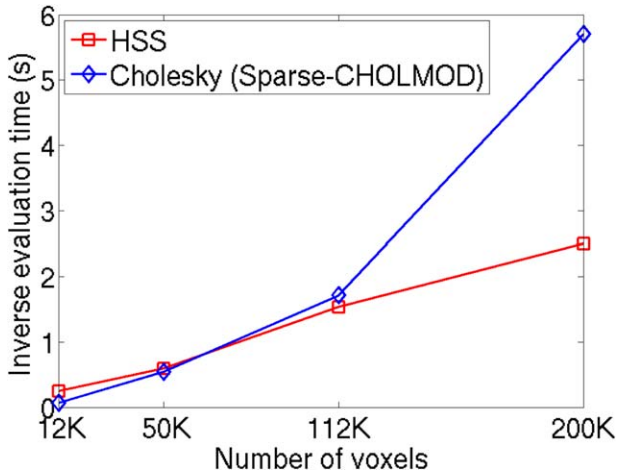


FIG. 2. Computational scaling with respect to image size for noniterative inverse methods. The time for a single inverse evaluation is shown for the optimized sparse Cholesky decomposition CHOLMOD and the HSS solver using a $10^{-6}$ tolerance. The matrix is associated with a $R = 3$ acceleration and 32 channels. The images range in size from $112 \times 112$ to $448 \times 448$.

implementation of the HSS solver will be faster for all image sizes. As we will demonstrate, the HSS evaluation of $A^{-1}$ has minimal dependency on the number of parallel imaging channels and the CS acceleration factor.

Finally, the precomputation trade-off for each method is shown above the respective flow diagrams in Figure 1. It is important to note that all of the CG methods can be optimized to exploit the Jacobi preconditioner, i.e., diag $(A)$. Thus, the *Matrix Free* method computes the least information prior to reconstruction and *HSS-Inverse* precomputes the most information (requiring an efficient representation for the inverse of the encoding matrix).

## METHODS

The focus of this work is on the application of a HSS solver for efficient SB reconstructions with SENSE parallel imaging. We evaluate the performance of our *HSS-Inverse* method against several CG-based approaches to highlight the computational trade-offs for reconstruction. The computational scaling for all approaches is analyzed with respect to the image size and the number of parallel imaging channels. The image accuracy for all methods is computed as RMSE against the complex coil combined images from the fully sampled data. Therefore, our results include computational aspects for the algorithms and analysis of the methods using the acquired data. Exhaustive sweeps of TV and soft-thresholding parameters were performed for "best case" accuracy. In practice, methods such as (13,14) could be used. As both the CG and HSS solvers have controllable accuracy, we choose a typical $10^{-6}$ criteria for all methods to ensure consistent results across the reconstructions.

To accurately compare the different CS approaches, multicontrast in vivo data were acquired from a healthy volunteer subject to institutionally approved protocol consent. The data were acquired on a 3T Siemens Trio with the standard Siemens 32-channel head array coil. T2-weighted and fluid attenuated inversion recovery (FLAIR) images were acquired with a $224 \times 224\,\mathrm{mm}^2$ field of view, across 35 slices with a 30% distance factor. The T2-weighted scan uses a turbo spin echo sequence with imaging parameters pulse repetition time (TR) = 6.1 s, echo time (TE) = 98 ms, flip angle = 150°, and a resolution of $0.5 \times 0.5 \times 3.0\,\mathrm{mm}^3$, with a matrix size of $448 \times 448$. The FLAIR scan uses a turbo spin echo sequence with an inversion pulse and imaging parameters TR = 9.0 s, TE = 90 ms, inversion time (TI) = 2.5 s, flip angle = 150°, and a resolution of $0.9 \times 0.9 \times 3.0\,\mathrm{mm}^3$, with a matrix size of $256 \times 256$. The fully sampled uncombined complex k-space data were retrospectively undersampled for all computational experiments. To examine the computational scaling of the CS reconstruction algorithms, datasets of consistent size were generated across the multiple imaging contrasts. Where applicable, matrix sizes of $112 \times 112, 168 \times 168, 224 \times 224$, and $280 \times 280$ were constructed by down-sampling the coil data. We utilize these images to represent resolutions of $0.8, 1.0, 1.33$, and 2.0 mm for the same field of view. In this work, data from two representative imaging slices will be used as test cases for the performance of the reconstruction methods. Sensitivity maps were created using JSENSE (15) estimation and used for all reconstructions. A 10th -order polynomial was used to fit the sensitivity profiles during the iterative JSENSE sensitivity map estimation. The polynomial fitting was performed only across a masked region of the brain.

We consider random undersampling schemes based on the method described in (3), where a variable polynomial density factor of 6 and a $1/R$ partial distance was used to generate each of the one-dimensional (1D) undersampling patterns. The results of the CS reconstructions are compared to the SENSE reconstruction using fully sampled data and the assumed sensitivity maps. In this work, our error metric is defined as the normalized root mean squared error against the SENSE images for any of the contrasts. All algorithms were implemented in MATLAB and numerical experiments were performed on AMD Opteron 6282 SE 2.6 GHz processors. MATLAB was run in single threaded mode to give accurate computational scaling for all of the methods. The standard MATLAB implementation of CG was used with the sparse Jacobi preconditioner. When investigating the impact of coil compression for CG-based approaches, the geometric coil compression MATLAB code associated with (11) was used. The MATLAB implemented HSS solver was provided through a request of the authors of (1). Similar to the tree-based FFT algorithm, the HSS solver used in this work can be easily made parallel for improved performance. We consider this to be future work for the proposed *HSS-Inverse* method.

## RESULTS

Figure 3 shows the *HSS-Inverse* reconstructed images and error for T2 and FLAIR imaging contrasts at resolutions of $0.8 \times 0.8 \times 3.0\,\mathrm{mm}^3$ and $1.0 \times 1.0 \times 3.0\,\mathrm{mm}^3$, respectively. In addition, Figure 3 illustrates the effect of channel compression on the reconstruction error. Figure 3a shows the $R = 1$ sensitivity combined images from the fully sampled 32-channel T2 data. The reconstructed images and error are shown below for 32 and 8-channel undersampled data, assuming $R = 3$ and 4 accelerations, respectively. The coil compression method (11) is used to project the 32-channel undersampled data to eight effective channels. This projection is also applied to the sensitivity maps. The dynamic range for the error images is scaled to 1/8 of the $R = 1$ images seen in Figure 3a. Similar results are shown for the FLAIR images in Figure 3b. When considering the original 32 channels, the $R = 3$ and 4 reconstructed T2 images had errors of 6.8 and 9.8% for the middle slice and 6.0 and 8.9% for the upper slice. The reconstructed FLAIR images had errors of 8.0 and 9.3% for the middle slice and 7.1 and 8.3% for the upper slice. Error for the eight-channel compressed reconstruction is measured against the fully sampled combination across the original 32 channels. Thus, this includes the error due to coil compression loss which was under 0.2% across all cases considered in this work. As alluded to above, the tolerance for the linear solvers used in each CS strategy leads to nearly identical reconstructions. Figure 4 shows the relative difference between the images reconstructed using the *Matrix Free* and *HSS-Inverse* methods. These extremely small differences are calculated by first subtracting the

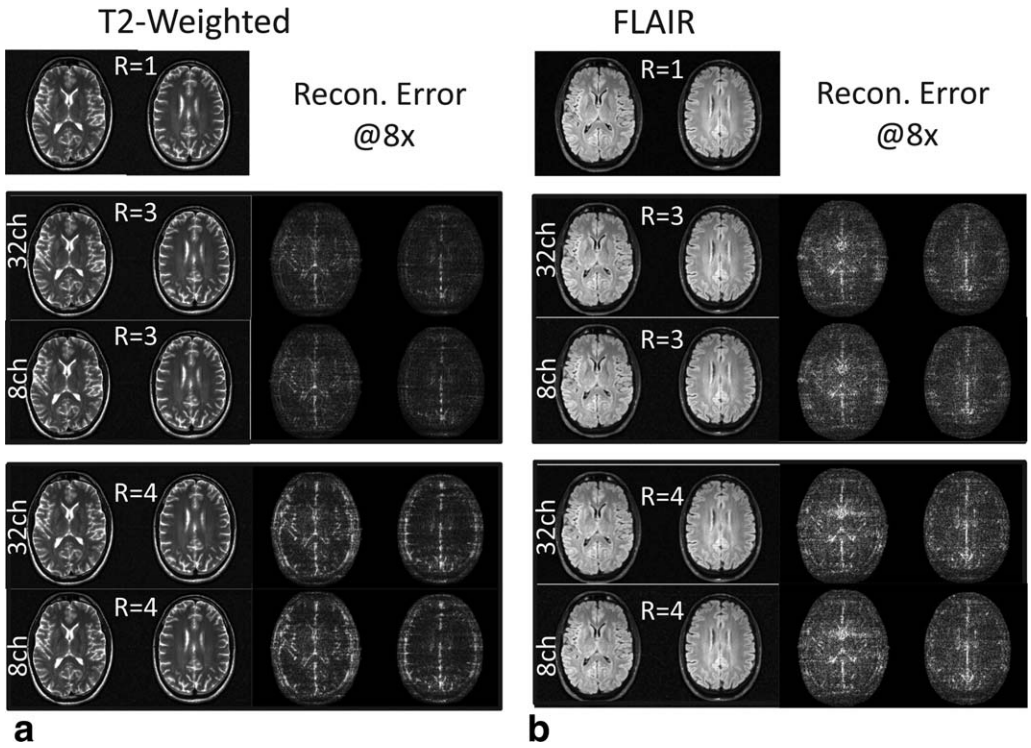


FIG. 3. CS+SENSE reconstructed images and error for T2 and FLAIR imaging contrasts. The dynamic range for the error images is scaled to 1/8 of the fully sampled and sensitivity combined ground truth images. (**a)** shows the $R = 1$ sensitivity combined images for the T2 contrast at a resolution of $0.8 \times 0.8 \times 3\,\text{mm}^3$. The reconstructed images and error are shown below for $R = 3$ and 4 accelerations using either the coil compressed eight-channel undersampled data or the full 32-channel data. Similar results are shown for the FLAIR images at a resolution of $1.0 \times 1.0 \times 3\,\text{mm}^3$ in (**b**).

images and then scaling each voxel by the image intensity.

Figure 5 illustrates the computational scaling of several SB optimization techniques with respect to image size. The *Matrix Free* and *Matrix* methods rely on preconditioned CG to solve (4) and our *HSS-Inverse* method uses the HSS direct solver, see Figure 1 for algorithm flow-diagrams. To ensure consistent reconstruction error all numerical approaches assume a $10^{-6}$ tolerance for the solution (4). The times reported in Figure 5 correspond to five iterations of SB with a TV weighting $\beta = 3 \times 10^{-3}$ and soft-thresholding $\epsilon = 2 \times 10^{-1}$. The Jacobi preconditioner is used for all CG methods. The use of Cartesian optimized coil compression from 32 to 8 channels is

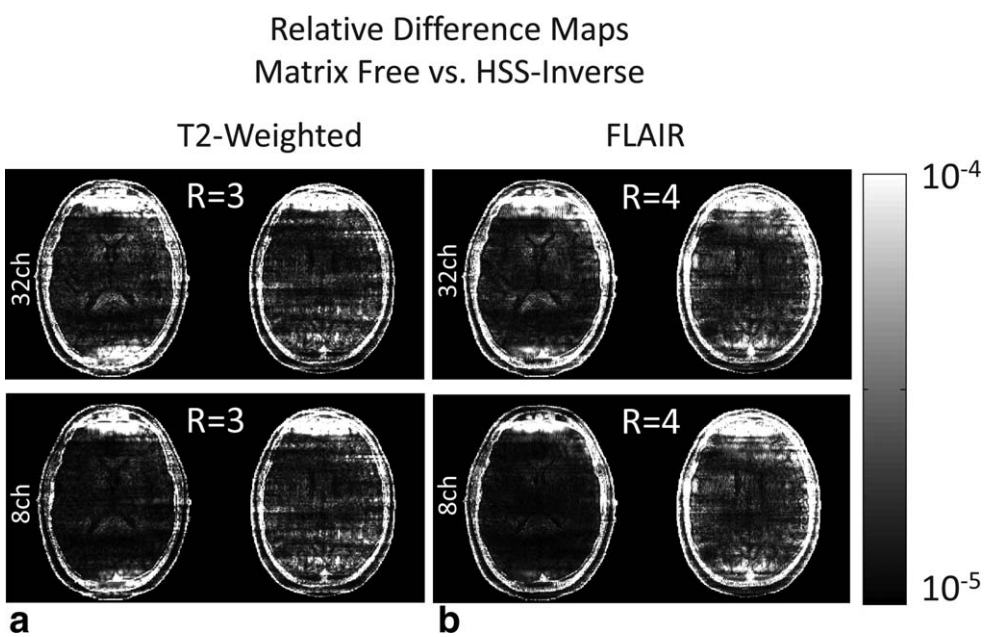


FIG. 4. Relative difference in CS+SENSE reconstructed images for T2 and FLAIR imaging contrasts between the *Matrix Free* and *HSS-Inverse* methods. The relative difference is shown for $R = 3$ and 4 accelerations using either the coil compressed eight-channel undersampled data or the full 32-channel data.

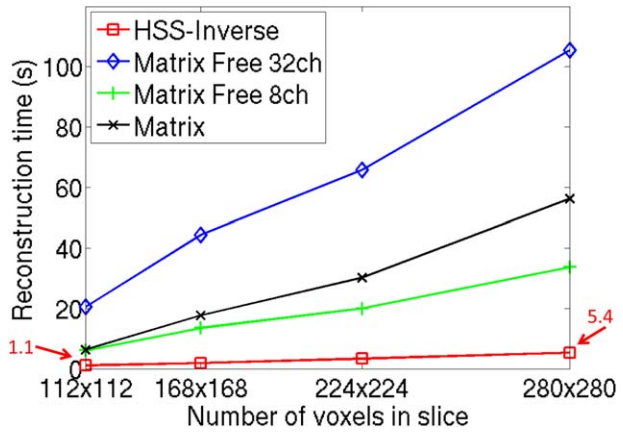


FIG. 5. Computational scaling with respect to image size for CG- and HSS-based reconstruction methods, see Figure 1 for algorithm flow-diagrams. $R=3$ acceleration is applied to the T2 weighted images. A $10^{-6}$ tolerance is assumed for all algorithms to ensure consistent final image error. All methods include five iterations of SB with a TV weighting $\beta = 3 \times 10^{-3}$ and soft-thresholding $\epsilon = 2 \times 10^{-1}$. The Jacobi preconditioner is used for all CG methods. The use of Cartesian optimized coil compression from 32 to 8 channels is explored for the *Matrix Free* method. The smallest and largest reconstruction times for *HSS-Inverse* are identified with arrows.

explored for the *Matrix Free* method. The *HSS-Inverse* method had times of 1.1 and 5.4 s for in-plane resolutions of $2 \times 2$ to $0.8 \times 0.8\text{mm}^2$. With the use of 4× channel compression the *Matrix Free* method became the best performing alternative to *HSS-Inverse*. It is important to note that the *HSS-Inverse* preprocessing time is not included in the reconstruction time as this calculation is independent of the acquired data and can be precomputed. It is, however, noted that the model inversion time is small and increased linearly from 5 to 116 s for these image sizes [and can be computed in parallel (1)].

Finally, Figure 6 demonstrates the lack of dependence of the *HSS-Inverse* method on the number of parallel imaging channels and acceleration factor. Here, reconstruction parameters consistent with the results shown in Figure 5 are used. $R = 2, 3, \text{and } 4$ accelerations are examined across in-plane resolutions from $2 \times 2$ to $0.8 \times 0.8\text{mm}^2$. The deviation in reconstruction time for *HSS-Inverse* was under 0.7 s for all cases considered. This small deviation in time should be considered a constant based on the numerical conditioning of the matrix $A$. The method from Ref. (1) automatically accounts for numerical stability to grantee accuracy for all possible linear system solutions. Alternatively, the *Matrix Free* computation time will increase linearly as the number of channels increases, see Figure 1.

## DISCUSSION AND CONCLUSIONS

In this work, we propose an efficient CS reconstruction strategy for MRI assuming SENSE parallel imaging. The proposed *HSS-Inverse* method exploits the fact that the SB framework produces a series of least squares problems with a fixed reconstruction operator. *HSS-Inverse* computationally outperformed all methods at all image sizes, with a reconstruction time of only 5.4 s for a 280 ×280 image with 32 channels. When considering the full 32 channels, the speedup of *Matrix* compared to *Matrix Free* reduced from 3.3× to 1.9× as the resolution increased. This is due to the superior computational scaling of the FFT operation for the *Matrix Free* method. Compression from 32 to 8 channels was required for the *Matrix Free* method to outperform the *Matrix* method at all of the resolutions. The speedup for the 32-channel *HSS-Inverse* over the eight-channel *Matrix Free* increases from 5.7× to 6.3× when the in-plane voxel size was reduced from $2 \times 2$ to $0.8 \times 0.8\,\text{mm}^2$. This is a result of the linear scaling of (1) and the nonlinear scaling for all other methods. In addition, we demonstrate minimal computational dependency with respect to both the acceleration factor and the number of parallel imaging channels for the proposed *HSS-Inverse* method. Given the dependence of the CG-based *Matrix Free* method on channel count, we expect this speedup to increase when considering larger array coils as additional compressed channels will be required for similar accuracy. It is important to note that the *Matrix Free* methods also utilize highly optimized FFT code and by reimplementing our MATLAB code into a lower level programming language we expect to see further improvement for the speedup.

HSS solvers have been previously used to efficiently solve large-scale 2D and three-dimensional (3D) problems in applied mathematics and physics. Linear-time scaling has been proven for many relevant 2D problems and $\mathcal{O}(N^{4/3})$ scaling for 3D problems. In this work, we have shown the applicability of this compact modeling strategy toward SB operators assuming 1D random undersampling with in-plane resolutions up to $0.8 \times 0.8\,\text{mm}^2$. As was alluded to above, the efficiency of *HSS-Inverse* does not substantially change as the CS acceleration factor is increased which will ensure consistent reconstruction time regardless of the protocol. In addition, the HSS solver is noniterative and the computational time should not be significantly affected by choice of CS penalty parameters. In the context of

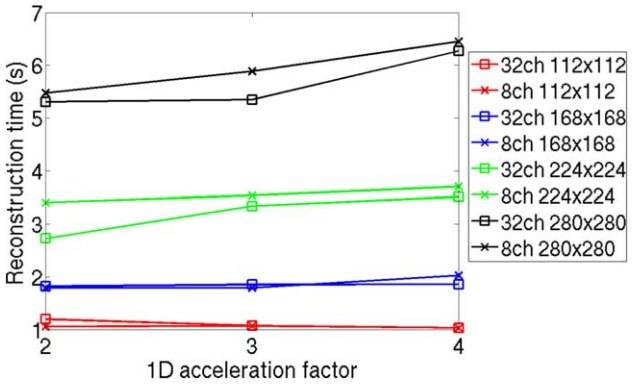


FIG. 6. Computational scaling of the *HSS-Inverse* method with respect to the number of parallel imaging channels and acceleration factor. A $10^{-6}$ tolerance is assumed for five iterations of SB with a TV weighting $\beta = 3 \times 10^{-3}$ and soft-thresholding $\epsilon = 2 \times 10^{-1}$. Cartesian optimized coil compression is used to reduce from 32 to 8 channels. $R = 2, 3,$ and 4 undersampling is examined.

prespecified MRI acquisition protocols, many factors for the *HSS-Inverse* method can be precomputed and should enable clinically relevant reconstruction times, e.g., the computation of the inverse encoding matrix can be computed as part of a separate adjustment scan.

We have introduced the idea of compact representations for the inverse of CS+SENSE reconstruction operators. This is accomplished through the use of a noniterative HSS numerical technique. The methods presented here should be applicable to many reconstruction operators that rely on locality of interactions, e.g., wavelet transformations (16) and GRAPPA based parallel imaging (17,18). Finally, the proposed *HSS-Inverse* method should be amendable to computationally demanding applications such as cardiac imaging (10) wherein the problem size can become very large due to the additional time dimension.

## REFERENCES


1. Xia J, Chandrasekaran S, Gu M, Li XS. Superfast multifrontal method for large structured linear systems of equations. SIAM J Matrix Anal A 2009;31:1382–1411.
2. Chen Y, Davis T, Hager W, Rajamanickam S. Algorithm 887: CHOLMOD, supernodal sparse cholesky factorization and update/downdate. ACM Trans Math Softw 2008;35:22.
3. Lustig M, Donoho D, Pauly JM. Sparse MRI: the application of compressed sensing for rapid MR imaging. Magn Reson Med 2007;58:1182–1195.
4. Pruessmann KP, Weiger M, Scheidegger MB, Boesiger P. SENSE: sensitivity encoding for fast MRI. Magn Reson Med 1999;42:952–962.
5. Block KT, Uecker M, Frahm J. Undersampled radial MRI with multiple coils. Iterative image reconstruction using a total variation constraint. Magn Reson Med 2007;57:1086–1098.
6. Liu B, King K, Steckner M, Xie J, Sheng J, Ying L. Regularized sensitivity encoding (SENSE) reconstruction using Bregman iterations. Magn Reson Med 2009;61:145–152.
7. Liang D, Liu B, Wang J, Ying L. Accelerating SENSE using compressed sensing. Magn Reson Med 2009;62:1574–1584.
8. Goldstein T, Osher S. The split Bregman method for L1-regularized problems. SIAM J Imaging Sci 2009;2:323–343.
9. Ramani S, Fessler J. An accelerated iterative reweighted least squares algorithm for compressed sensing MRI. In IEEE International Symposium on Biomedical Imaging, Rotterdam, Netherlands, 2010. pp. 257–260.
10. Otazo R, Kim D, Axel L, Sodickson DK. Combination of compressed sensing and parallel imaging for highly accelerated first-pass cardiac perfusion MRI. Magn Reson Med 2010;64:767–776.
11. Zhang T, Pauly JM, Vasanawala SS, Lustig M. Coil compression for accelerated imaging with Cartesian sampling. Magn Reson Med 2013; 69:571–582.
12. Saad Y. Iterative methods for sparse linear systems, 2nd ed. Philadelphia, PA: SIAM; 2003. 547 p.
13. Hansen P, O'Leary D. The use of L-curve in the regularization of discrete ill-posed problems. SIAM J Sci Comput 1993;14:1487–1503.
14. Weller DS, Ramani, S Nielsen J, Fessler J. Monte Carlo SURE-based parameter selection for parallel magnetic resonance imaging reconstruction. Magn Reson Med 2014;71:1760–1770.
15. Ying L, Sheng J. Joint image reconstruction and sensitivity estimation in SENSE (JSENSE). Magn Reson Med 2007;57:1196–1202.
16. Lustig M, Pauly JM. SPIRiT: iTerative self consistent parallel imaging reconstruction from arbitrary k-space sampling. Magn Reson Med 2010;64:457–471.
17. Griswold MA, Jakob PM, Heidemann RM, Nittka M, Jellus V, Wang J, Kiefer B, Haase A. Generalized autocalibrating partially parallel acquisitions (GRAPPA). Magn Reson Med 2002;47:1202–1210.
18. Weller DS, Polimeni JR, Grady L, Wald LL, Adalsteinsson E, Goyal VK. Denoising sparse images from GRAPPA using the nullspace method. Magn Reson Med 2012;68:1176–1189.